Average properties of geomagnetic storms in 1932–2009

O. S. Yakovchouk,[1,2] K. Mursula,[1] L. Holappa,[1] I. S. Veselovsky,[2,3] and A. Karinen[1]

Received 23 August 2011; revised 30 December 2011; accepted 4 January 2012; published 1 March 2012.

[1] We investigate the average properties of geomagnetic storms using the global and local Dxt indices at four Dst stations in 1932–2009. Imposing the condition of complete data availability during storms, our study includes 1268/362/134/59 storms with Dxt minimum less than −50/−100/−150/−200 nT, respectively. The global Dxt minima were, on an average, −94/−156/−216/−275 nT, while deepest storm-time local Dxt minima were −137/−214/−285/−350 nT. Accordingly, the local Dxt minima are typically 25–30% stronger than the global Dxt minima. The distribution of largest storm-time disturbances is strongly peaked at 18 local time (LT), challenging local midnight as the dominant ion source. Relative timing of local minima verifies that stations at earlier LT hour observe their minimum a couple of hours after the deepest minimum, in agreement with westward drift of ions. Storm-time maximum asymmetries were found to increase with storm intensity level from about 70 nT to 150 nT for −50 to −200 nT storms. However, strong storms are relatively more symmetric than weak storms when compared to the typical level of local disturbance. During individual storms the asymmetry can be more than 200 nT. The rate of evolution of storm-time asymmetry is found to be roughly twice as fast for large storms. We emphasize that the unique database of local Dxt indices proves to be very useful in studying the average spatial distribution and temporal evolution of storms.

Citation: Yakovchouk, O. S., K. Mursula, L. Holappa, I. S. Veselovsky, and A. Karinen (2012), Average properties of geomagnetic storms in 1932–2009, *J. Geophys. Res.*, *117*, A03201, doi:10.1029/2011JA017093.

1. Introduction

[2] During geomagnetic storms a large amount of energy is injected into the inner magnetosphere due to a long period of steady or fluctuating southward directed interplanetary magnetic field. Such special periods are produced especially during interplanetary coronal mass ejections (CME) and corotating interaction regions (CIR) driven by high speed streams [see, e.g., *Gonzalez et al.*, 1999; *Kamide and Maltsev*, 2007]. As a consequence, the flux of energetic particles is suddenly and significantly increased over a range of fairly low L-shells, typically L = 3-6. The Dst index [*Sugiura*, 1964] was developed to measure the magnitude of the ring-shaped current produced by these newly accelerated energetic particles. The Dst index is constructed from the large negative deflection in the horizontal magnetic field caused by the westward directed electric current formed by the westward drift of energetic, positively charged ions. However, it is known that other current systems, in particular the tail current, also contribute to the Dst index, at least during the storm main phase [see, e.g., *Burton et al.*, 1975; *Campbell*, 1996, 2004]. It is also known by now that the ring current is quite asymmetric and that the largest storm-time disturbances are rather localized in longitude [see, e.g., *Lui et al.*, 1987; *Liemohn et al.*, 2001; *Takalo and Mursula*, 2001; *Huttunen et al.*, 2006]. The asymmetry is most typically caused by ions drifting westward around the dusk sector toward the noon, staying partly on open drift shells and therefore being guided out through the dayside magnetopause. Accordingly, the morning sector is only partly filled with drifting ions.

[3] The Dst index is calculated from the observations of the horizontal magnetic field at four low- to midlatitude stations (Hermanus, HER; Honolulu, HON; Kakioka, KAK; San Juan, SJG; for coordinates see Table 1) according to the recipe developed in the 1960s [see, e.g., *Sugiura*, 1964; *Sugiura and Kamei*, 1991]. The Dst index is maintained by the World Data center for Geomagnetism, Kyoto (http://wdc.kugi.kyoto-u.ac.jp/dstdir/) since the International Geophysical Year 1957. More recently, several groups [*Karinen and Mursula*, 2005; *Xu et al.*, 2008; *Love and Gannon*, 2009] have started producing alternate versions of the Dst index or its proxies, trying, e.g., to modify or correct some deficiencies or problems of the "official" Dst index. We have reconstructed the Dst index using the original Dst derivation recipe as closely as possible [*Karinen and Mursula*, 2005, 2006], except that the local disturbances were normalized by the cosine of station's geomagnetic latitude [*Mursula et al.*, 2008]. This index is called the Dxt index in order to distinguish it from the Kyoto Dst index. One of the main aims of that work was to extract the local disturbances contributing to the global Dxt index (to be called here the local Dxt indices; the global Dxt index being

[1]Department of Physics, University of Oulu, Oulu, Finland.
[2]Institute of Nuclear Physics, Moscow State University, Moscow, Russia.
[3]Space Research Institute, Russian Academy of Sciences, Moscow, Russia.

0148-0227/12/2011JA017093

Table 1. Geographical and Geomagnetic Coordinates of the Dst Magnetic Stations According to IGRF 2000 Model[a]

	Geographic		Geomagnetic	
Station, IAGA Code	Latitude	Longitude	Latitude	Longitude
Cape Town, CTO	−34.57°	18.28°	−33.89°	82.73°
Hermanus, HER	−34.42°	19.23°	−33.91°	83.69°
Honolulu, HON	21.32°	202.00°	21.60°	269.45°
Kakioka, KAK	36.23°	140.18°	27.17°	208.50°
San Juan, SJG	18.12°	293.15°	28.53°	5.87°

[a]International Geomagnetism Reference Field (IGRF) (*International Association of Geomagnetism and Aeronomy*, Paris, 2000, available at http://www.iugg.org/IAGA/iaga_pages/pubs_prods).

the average of the four local Dxt indices) in addition to the global four-station average Dxt index, since corresponding local Dst indices are not available at Kyoto WDC. We will use here the global Dxt index and the local Dxt indices at the four Dst stations in order to study the temporal development and spatial structure of geomagnetic storms in more detail than possible only using the global index.

[4] As noted earlier [*Karinen and Mursula*, 2005], an exact reproduction of the original Dst index is not possible because of, e.g., the missing information on the treatment of data gaps. Moreover, the Dxt index is known to correct some errors in the original Dst index, thereby leading to differences between the two indices at certain times [*Karinen et al.*, 2002; *Karinen and Mursula*, 2005]. The Dxt index also extends the time span of the Dst index (which starts in 1957), by more than 25 years to start in 1932. This is possible by using the observations of the Cape Town station, which was the predecessor of Hermanus, with all other Dst stations starting their operations even earlier. Accordingly, the global and local Dxt indices present a homogeneous series of magnetospheric disturbances for nearly 80 years. Note also that, despite the above mentioned differences between the Dst and Dxt indices at certain times, the two indices are, overall, very similar and the average absolute difference between the two indices during the overlapping time interval 1957–2009 is only 3.2 nT. Therefore, most of the results obtained in this study using the Dxt indices would remain closely valid even if conducted based on the "official" Dst index, if the local Dst indices only were available.

[5] In this paper we use this unique database of local and global Dxt indices to study the average properties of storms of different intensity levels, in particular the average spatial distribution of the major disturbances and the average temporal evolution. This paper is organized as follows. In section 2 we describe the storm selection recipe and the basic statistics of storms. Section 3 presents two sample storms and their mutually quite different temporal evolutions. In section 4 we investigate the averages of local Dxt values during storms of different intensity levels. Section 5 presents the local time distribution of storm-time disturbances and section 6 discusses the UT time distribution of the global Dxt index and the time differences between the global and local indices. Section 7 discusses the storm-time asymmetries in detail. Finally, we give our conclusions in section 8.

2. Storm Selection and Number of Storms

[6] We have selected geomagnetic storms of four different (integral) intensity levels with the minimum value of the global Dxt index being less than −50/−100/−150/−200 nT. (For example, a storm with minimum Dxt index of −170 nT is included in the first three intensity levels, but not in the −200 nT level.) We first searched for all peaks at these levels during the whole period 1932–2009. From these we included only the deepest Dxt minima within a 6-day time interval, 72 hours (3 days) before and 72 hours after the peak hour. In this way storms with several minima (intensifications) were counted as one storm, within the intensity category determined by the deepest minimum. We also required that none of the four Dst stations should have any data gaps in the magnetic field H component in the time interval from −48 hours to +72 hours around the Dxt minimum hour. Setting this requirement on data availability at each station, we avoided the problem of data gaps in the local indices, and guaranteed that complete information is available for all storms from all four stations, leading to more systematic and reliable results.

[7] Using these criteria, we found 1268/362/134/59 storms in 1932–2009 with global Dxt minimum less than −50/−100/−150/−200 nT. Thus, the average annual number of storms with Dxt minimum below −50 nT was about 16 during this 78-year time interval. Out of these 476/123/49/19 storms occurred during the 24 year period 1932–1956 and 792/239/85/40 storms in the 52 year interval 1957–2009 when Dst index became available. Accordingly, there were relatively more storms/year (i.e., the storm rate was higher) in the earlier period. This is partly because of data gaps, which were more plentiful in the 1980s, partly because of the declining solar activity during the last decades. In order to compare the effect of the selection criteria on the number of storms, we have relaxed the condition of no gaps in Dst station data, finding that there were 1694/494/195/91 storms in 1932–2009, and 1121/342/133/66 storms in 1957–2009, if all available station data were used and the global index was calculated using those stations which have valid observations. (This policy slightly deviates from *Karinen and Mursula* [2005] who interpolated over small gaps.) Accordingly, the condition of gapless data did cause a notable reduction in the number of storms, the reduction percentage increasing slightly from about 25% to 35% with storm intensity in 1932–2009, and from about 30% to 40% in 1957–2009. The slightly larger reduction rates in 1957–2009 are in agreement with the above note of relatively more gaps in the latter period. Note also that the increase of reduction rates with storm intensity is in agreement with the idea that the gaps took place relatively more frequently during storm times. However, despite the reduction the number of storms remains quite large so that we can study the properties of storms even at different intensity levels.

[8] We also calculated the number of storms based on the minima of the Dst index in 1957–2009. Using only the 6-day separation condition, the numbers of Dst index storms were 1252/369/141/71, and using, in addition, the condition of no data gaps in Dst stations during the storms gave 885/257/87/41 storms. This shows a very similar reduction effect of about 30–40% when imposing the no-gap criteria, as seen in the Dxt index over the same time interval. Also, similarly, the reduction effect increases with storm intensity. Using the same criteria, the number of storms based on the Dst index or the Dxt index are quite similar, although there are some 5-10% more storms in the Dst index list. The larger number

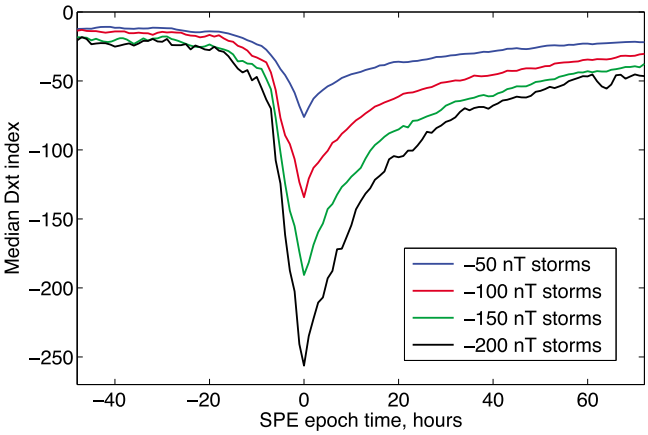

Figure 1. Superposed epoch median values of the hourly global Dxt indices for storms of different intensity levels. SPE zero time is the global Dxt minimum time.

of storms in the Dst list is, in the case of using all available data, at least partly due to the fact that some gaps in Dst index were filled with data from other than the four Dst stations, thus increasing the possibility that the additional station registered a large disturbance and made Dst slightly larger. However, since there are more storms in the Dst list even when imposing the no-gap condition (although the numbers are relatively more similar), this cannot be the only explanation, unless data from such additional stations were used even if data from all Dst stations would have been available. The latter possibility is plausible since data transfer in early times of the Dst index was not as fluent as today, and Kyoto WDC may indeed have had more gaps in Dst station data at the time when the Dst index was calculated. Unfortunately, we cannot verify this possibility since the local Dst indices are not available. However, the difference between the Dst and Dxt storm lists reduces with storm intensity and makes only 1 or 2 additional storms in the gapless Dst storm list for the two most intense storm categories. This shows that the large storms include relatively larger disturbances at all local times, whence it is less important for the global Dxt/Dst index where exactly the stations are located.

[9] For definiteness, the results presented in this study are based on storms found when using the global Dxt index and imposing the two conditions mentioned above (no data gaps in any of the Dst stations and a six-day separation between storms). Thus, no interpolation over index data gaps was needed, and all results are based on homogeneous and complete data. Figure 1 shows the average structure of storms of the four intensity levels within the time interval for which full data coverage was required (two days before and 3 days after Dxt minima). The storm curves are obtained by superposing the hourly storm-time indices in each intensity category and then taking the hourly median values. The hour with minimum Dxt was used as the superposed epoch (SPE) zero time. The Dxt minima of the SPE storms of Figure 1 were −76/−134/−191/−256 nT for storms with Dxt minimum below −50/−100/−150/−200 nT. Understandably, at all intensity levels the SPE Dxt minima were below the limit. However, the amount by which the SPE minima went below the limit decreased from 52% to 28% with storm intensity.

3. Sample Storm Events

[10] We show here two examples of storms, depicting the global Dst and Dxt indices and the local Dxt indices at the four Dst stations. The minimum values of these six indices and their UT and local time hours are given in Table 2 for the two storms. The selection consists of and one major storm (Dst minimum = −301 nT) in July 2000 and one intermediate storm (Dst minimum = −106 nT) in July 2003. As can be seen in Table 2, the Dst and Dxt minima and their UT hours agree well for both storms. One can also see that two local storm-time Dxt minima (HER and SJG) are clearly below the global Dxt minimum for the July 2000 storm, one above (KAK) and one almost equal to Dxt minimum (HON). For July 2003 storm, one local Dxt minimum (HON) was by roughly 35% below the global Dxt minimum, others attaining a roughly similar value as the global Dxt minimum. We will now discuss the time evolution of these storms, as observed at the four Dst stations. The samples show that the storm evolution can be quite similar in the different stations (local time sectors) during some storms, but quite different in others.

[11] Figure 2 depicts the major storm of July 2000. During this storm, the four Dst stations depict a closely similar temporal evolution during the whole storm time, despite the different absolute levels. This is particularly valid for HER, HON and KAK, while SJG depicts the largest disturbance among the four stations at 22 UT, i.e., 2–3 hours earlier than other stations (see Table 2). The minimum of the global Dxt is found at 0 UT. During this storm the momentary asymmetry (the largest hourly difference between any two stations; see Figure 2) is mainly due to the difference in absolute levels of local disturbances, rather than the small timing difference between the local minima. The asymmetry has its maximum at 23 UT, i.e., one hour before the Dxt minimum. The largest disturbance of SJG takes place at 18 LT, in a good agreement with the statistical location of the largest disturbance (see later). This storm is driven by a very regular, almost sinusoidal variation of the solar wind electric field Ey component, which reaches its maximum of about 50 mV/m four hours before Dxt minimum in the middle of the main phase (see Figure 2). The variation of Ey (dominated by variations in IMF Bz; for a detailed study of this event, see *Lepping et al.* [2001]) reflects the internal

Table 2. Minima of the Global Dst and Dxt and the Four Local Dxt Indices as Well as Their UT and LT Hours for the Two Sample Storms

	HER	HON	KAK	SJG	Dxt	Dst
July 15–16, 2000						
Minimum value (nT)	−330	−301	−250	−376	−299	−301
Minimum UT hour	0	1	1	22	0	0
Minimum LT hour	1	14	10	18		
July 11–12, 2003						
Minimum value (nT)	−103	−140	−102	−102	−106	−106
Minimum UT hour	18	5	5	1	5	5
Minimum LT hour	19	18	14	21		

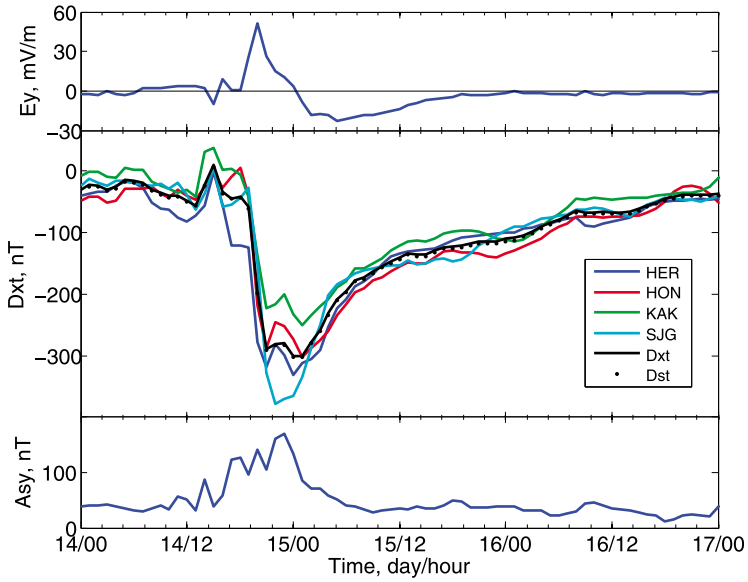

Figure 2. July 15–16, 2000, storm with Dxt minimum of −299 nT at 0 UT. (top) Solar wind electric field y-component (Ey). (middle) Global Dxt (black line), Dst (dots) and the four Dst stations (HER blue, HON red, KAK green, SJG light blue). (bottom) Momentary asymmetry. Time spans from −48 to +72 hours around Dxt minimum time.

structure of the magnetic cloud that drives this storm (for more information on CME storms, see, e.g., *Tsurutani and Gonzalez* [1997], *Zhang et al.* [2007], *Echer et al.* [2008], and *Gopalswamy* [2010]). Clearly, the rapid, coherent evolution at all local times during this storm is due to this specific temporal development of the driver.

[12] As noted above, the other three Dst stations at widely different LT sectors attain their largest Dxt indices almost simultaneously with SJG, not only after reaching the 18 LT sector where SJG detected the largest disturbance. In fact, the large disturbance at 18 LT must have largely decayed before any other station reached that sector. Therefore, the partial ring current region of maximum disturbance at 18 LT must have lasted only a few hours. The westward drift of ions is supported by the heights of maxima decreasing from SJG to HON and KAK, and their relative timing. However, it cannot explain the fact that HER sees at 2 LT a larger disturbance than HON or KAK, even one hour earlier than these two stations but two hours later than SJG. Clearly, if there was one main location of ion injection, it was not in the post-midnight sector but rather between late afternoon and midnight. We note that the double-minimum structure observed in three stations is most likely due to a moderate pressure pulse taking place at this time, increasing the H-component in all other stations except in SJG at 18LT sector. Without this disturbance the development at all four stations would be even more similar.

[13] A very different storm was observed in July, 2003 (see Figure 3). The overall evolution of this storm was much slower than in July 2000 storm, and the maximum value of

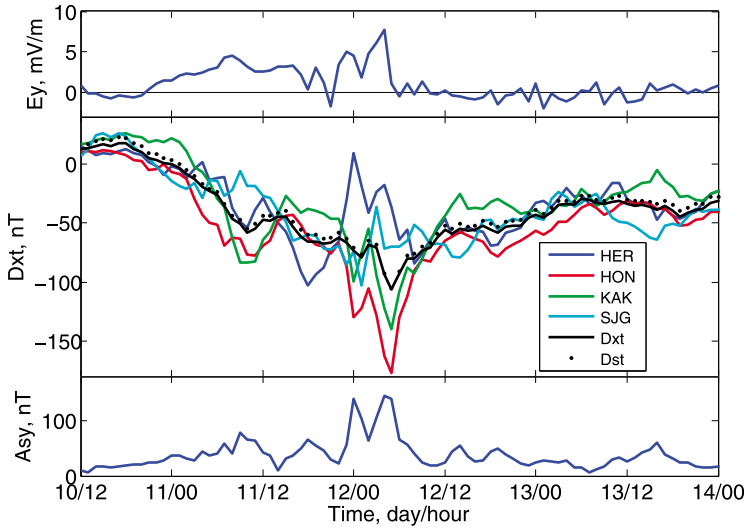

Figure 3. July 11–12, 2003, storm with Dxt minimum of −106 nT at 5 UT. Presentation as in Figure 2.

Table 3. Average Values Local and Global Dxt Minima, and the Deepest and Weakest Storm-Time Minima for the Different Storm Levels in 1932–2009[a]

	HER	HON	KAK	SJG	Deepest	Weakest	Dxt
Dxt ≤ −50 nT storms	−109	−120	−104	−118	−137	−88	−94
Dxt ≤ −100 nT storms	−172	−188	−169	−182	−214	−143	−156
Dxt ≤ −150 nT storms	−234	−255	−234	−242	−285	−196	−216
Dxt ≤ −200 nT storms	−295	−313	−289	−298	−350	−243	−275

[a]All numbers are in units of nT.

Ey remained significantly weaker. Connected with the first Ey maximum in the late morning of July 11, HON and KAK first, and later HER, observed Dxt minima while in the afternoon sector. For HER, this became to be its storm-time minimum and, even if Ey increased considerably larger in July 12, HER did not see a deeper minimum while in the post-midnight/early morning sector (0–6 LT). The storm-time Ey maximum in early July 12 led to simultaneous storm-time minima in HON and KAK, which were in the afternoon-evening sector at this time. The largest storm-time minimum was observed at HON in the 18 LT sector, again in a good agreement with statistical results (see later). The global Dxt minimum was also attained at this time, even if SJG in the post-midnight sector and especially HER in the morning sector showed rather weak Dxt values. (SJG depicted a very smooth overall evolution with minimum in early July 12 at 21 LT sector, at the time when Ey had a local minimum.)

[14] The July 12 storm depicts only vague direct evidence for the westward drift of ions. If this takes place, only a small amount of ions would reach the morning sector, since HER and SJG detect rather weak local minima after the global Dxt minimum. The ions may have located at higher L-shells, being guided out of the system while drifting around the Earth mostly on open drift shells. This storm was driven by a high-speed stream [*Richardson et al.*, 2006] (for a review of HSS related activity, see, e.g., *Tsurutani et al.* [2006]). In this storm the relative importance of the 18 LT sector is even more significant than in July 2000 storm. This also leads to an asymmetry (also depicted in Figure 3), which is relatively larger when compared to the global Dxt minima (and roughly equally large even in absolute value) than in July 2000 storm. While the global Dxt minimum in July 2003 storm was only −106 nT, the momentary asymmetry during global Dxt minimum hour was 140 nT. These facts demonstrate that the view based only on the global Dxt minimum is very partial, and that the evolution of this CIR driven storm was in many respects quite different from the evolution of the CME driven July 2000 storm.

4. Average Local Dxt Indices

[15] Table 3 shows the values of the average local Dxt minima at the four Dst stations during all storms at four intensity levels in 1932–2009. Table 3 depicts the fact that Honolulu reaches, on an average, slightly larger disturbances and KAK smaller than all other stations. Although the reason to this difference is now understood to be due to the quiet-day treatment in the Dst index recipe [*Mursula et al.*, 2011], we prefer not to correct for this difference here, in order to keep the results as close to the Dst index as possible. Moreover, the station differences are rather small when compared to the overall scale of storm disturbances, and even below the statistical fluctuations among the local Dxt indices at any storm intensity level, as will be shown later.

[16] Table 3 shows that the global Dxt minima are, on an average, less negative than all local Dxt minima for all intensity levels. In fact, the average values of local Dxt minima are 19/22/25/24 nT more negative than the global Dxt index minima for the four intensity levels. (We also note that the averages of global Dst minima are almost the same as for the Dxt index at all storm levels, when using the same time interval; these are not shown in Table 3, which depicts the values for 1932–2009.) Table 3 also includes the mean values of the deepest (most disturbed) and the weakest (least disturbed) storm-time local Dxt minimum. The former show that, typically, the deepest storm-time local minimum (−137/−214/−285/−350 nT) is about 31/27/24/21% deeper than the global Dxt minimum of the same storm. Although in individual storms this difference can be much larger, these percentages give the average rates by which the global Dxt/Dst index underestimates the largest local disturbance. Note also that, interestingly, these rates systematically decrease with storm intensity, supporting the view [*Richardson et al.*, 2006] that the weaker storms, which include a considerable fraction of CIR related storms, are relatively more asymmetric than the stronger storms, which are mostly CME driven.

[17] We have plotted in Figure 4 the local Dxt indices of the four stations for each storm as a function of the global Dxt index of the storm. Figure 4 (top) depicts the momentary Dxt values at each station during the hour of the global Dxt minimum. On the other hand, Figure 4 (bottom) depicts the local storm-time Dxt minima at each station during each storm, irrespective of the relative timing between the station Dxt minimum and the global Dxt minimum. Note that the Dxt indices of the four stations depict the small systematic differences mentioned above (HON largest, KAK smallest). However, as seen in Figure 4, these differences are much smaller than the spread of Dxt values for any station at any intensity level.

[18] The scatter in local Dxt indices at the time of global Dxt minima (Figure 4, top) is about 180 nT. So, e.g., for global Dxt minimum = −100 nT storms the local Dxt indices can range from slightly negative to almost −200 nT. On the other hand, when taking the storm-time Dxt minima at each station (Figure 4, bottom), the scatter is smaller, about 130 nT. This is because the smallest (momentary) local disturbances are removed from the distribution. For example, for −100 nT storms, the highest (smallest in absolute value) local Dxt minima are about −60 nT. However, the largest disturbances in Figure 4 (bottom) are not much larger than in Figure 4 (top), since the global Dxt minimum occurs at a time when at least one station attains its maximum disturbance (see also the sample storms). Interestingly, the spread of the two distributions increases only very slowly with storm intensity and remains almost constant below −100 nT. (However, quantile limits increase with intensity slightly faster; not shown.) In case of Figure 4 (top), this indicates that with increasing storm intensity all local time sectors get more and more disturbed by the end of the storm main phase. The constant spread in Figure 4 (bottom), i.e.,

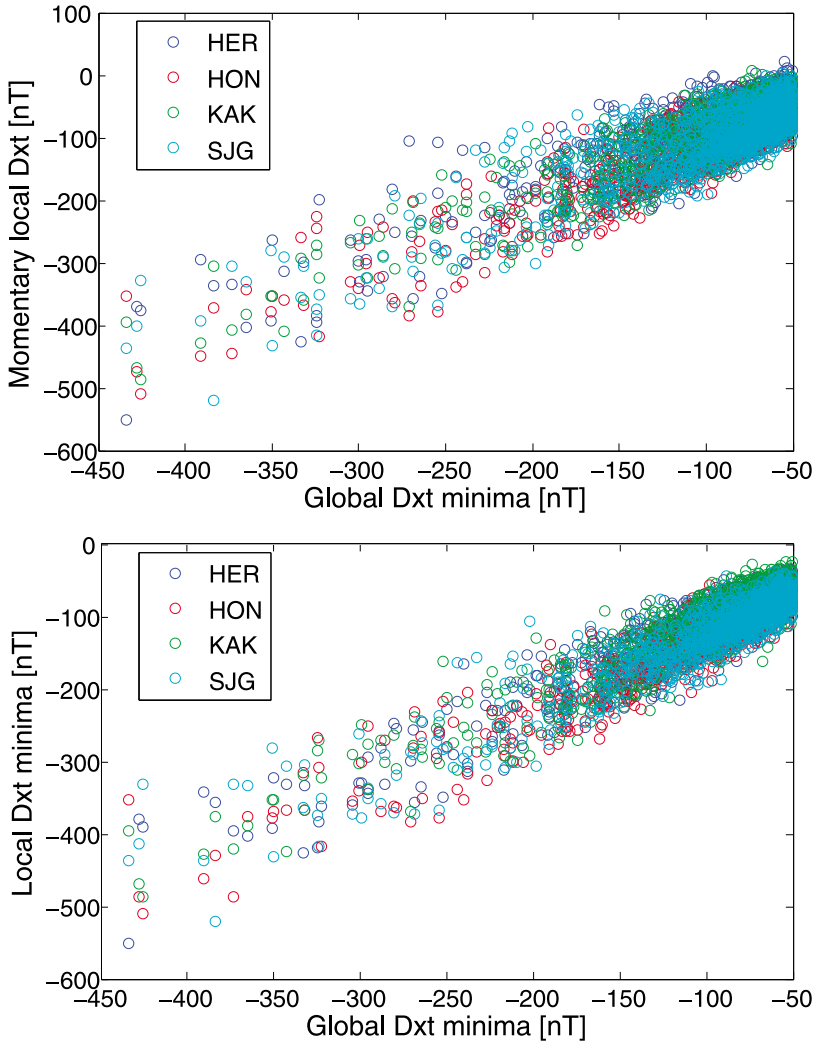

Figure 4. Local Dxt indices for all stations as a function of the global Dxt index of the storm. (top) Momentary Dxt values during the hour of the minimum global Dxt index; (bottom) storm-time local Dxt minima.

the fact that the difference between maximum local disturbances remains rather constant, is in agreement with the view that storms become relatively more symmetric with increasing intensity. (We will return to Figure 4 later when discussing storm asymmetry.)

5. Local Time Distributions

[19] Figure 5 depicts the local time distribution of storm-time minima of local Dxt indices at each station for Dxt minimum less than −100 nT storms. The distribution reproduces the well-known preponderance of the largest disturbances in the evening LT sector and the related ring current local time asymmetry [see, e.g., *Takalo and Mursula*, 2001; *Liemohn et al.*, 2001; *Le et al.*, 2004; *Weygand and McPherron*, 2006; *Huttunen et al.*, 2006; *Kalegaev et al.*, 2008; *Love and Gannon*, 2009]. This was also demonstrated by the sample storms discussed above. For all three northern hemisphere stations the peak of distribution is found at 18 LT, and for HER at 19 LT. The half width of the distribution is about 10 hours from 12 LT to 22 LT, clearly excluding midnight as the location of the largest disturbances. Note also that distributions are not symmetric around 18 LT but tend to have a sharper edge toward midnight (i.e., eastward) than toward noon (westward). In fact, this corresponds to the westward drift of storm-time ions, as will become more evident later.

[20] Note also that HER distribution in Figure 5 slightly deviates from the distribution of the three other stations, depicting a side-maximum at 10 LT. This side-maximum mainly corresponds to those storms where KAK, the first station ahead of HER in local time is in the evening sector of maximum disturbance. In order to demonstrate this, we have taken all those Dxt minimum less than −100 nT storms where KAK was located in the 16–20 LT sector and observed the deepest storm-time local Dxt minimum there. Then we calculated the LT distribution of HER storm-time Dxt minima for these storms. Figure 6 shows that this conditioned HER distribution is centered at notably earlier LT hours, with the bulk of the distribution in 11–15 LT sector.

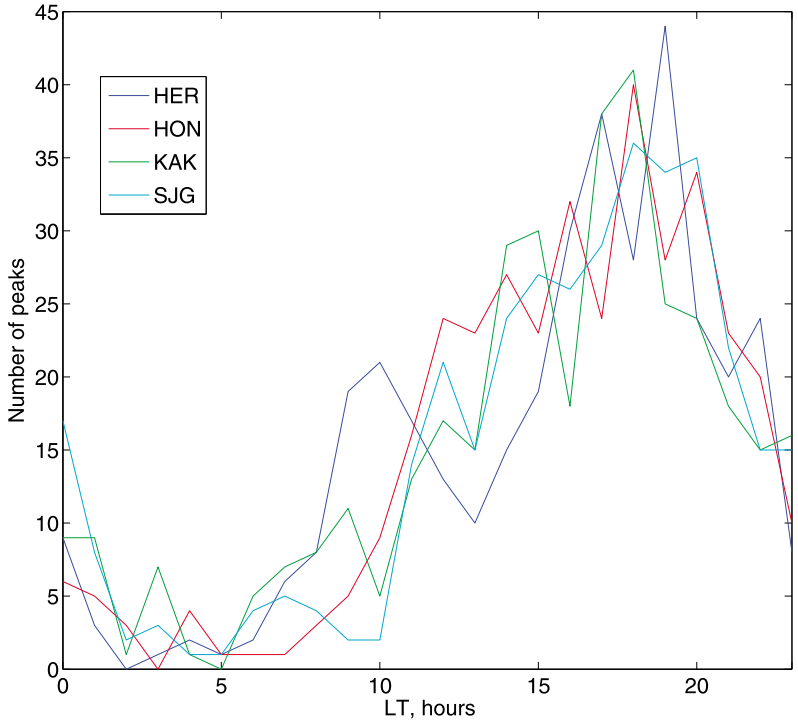

Figure 5. Local time distribution of storm-time minima of local Dxt indices at each Dst station for Dxt minimum less than −100 nT storms in 1932–2009.

There are hardly any storms around the 19 LT sector in Figure 6. Since HER is 7 hours behind KAK, the 16–20 LT sector in KAK corresponds to simultaneous 09–13 LT at HER. Accordingly, Figure 6 shows that there is a delay of about 2 hours, on an average, until the disturbance moves from KAK to HER. This gives the average motion of the energetic ions to traverse about 5 LT hours in about 2 hours. We note that similar changes in the conditioned LT distributions are found for the other stations as well. (We will analyze these changes in more detail in another publication.) Moreover, the side-maxima are found in the unconditioned distributions (like for HER in Figure 5) for all other stations at higher intensity levels.

[21] In order to further study the local time variation we determined, for each Dxt minimum less than −100 nT storm, the station that depicts the deepest local Dxt minimum, and plotted their LT distribution in Figure 7. This distribution is almost symmetric around the maximum at 18 LT, in notable difference to Figure 5. This is because the Dxt indices of the side-maxima at earlier LT hours (like those depicted for HER in Figures 5 and 6) are generally weaker than the indices of the station that is close to the 18 LT sector and are therefore dropped out from the distribution depicted in Figure 7. (Note also that the distribution of Figure 7 is fully independent of the small difference in the relative heights between the stations, which slightly affects the distributions in Figure 5.) In fact, Figure 7 presents the true LT distribution of the location of the largest disturbance observed by any of the Dst stations during the storm. Note also that the distribution in Figure 7 is very steep both toward the dayside and the night side. The ratio between the average number of Dxt minima at 18 LT and at 00 LT is more than 6. The steepness of the distribution toward midnight is problematic for the view that the disturbances observed in the evening sector are mainly due to ions that have been injected from the tail and drifted westward (for early papers, see, e.g., *Lyons and Williams* [1984] and *Williams* [1987]). This imposes a challenge for such observational results [see, e.g., *Le et al.*, 2004] or ring current models [see, e.g., *Jordanova et al.*, 2009; *Buzulukova et al.*, 2010] that find the largest disturbances in the night sector. On the other hand, this is in a good agreement with recent results [*Cash et al.*, 2010] of significant fluxes of oxygen ions appearing in the dusk sector during storm main phase. Related evidence for direct ion outflow from the ionosphere into the ring current in this sector has been found using

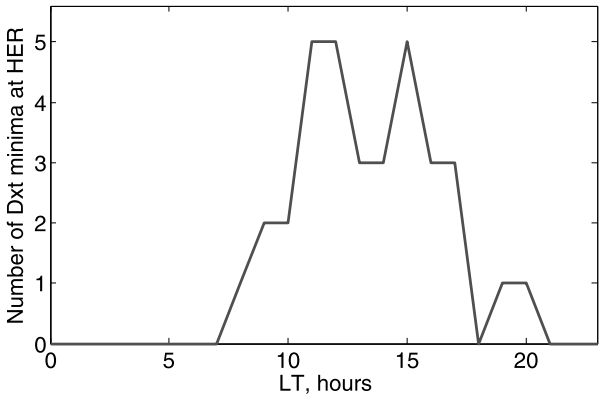

Figure 6. Local time distribution of local Dxt minima at HER during those −100 nT storms where KAK had the deepest storm-time Dxt minimum in the 16–20 LT sector.

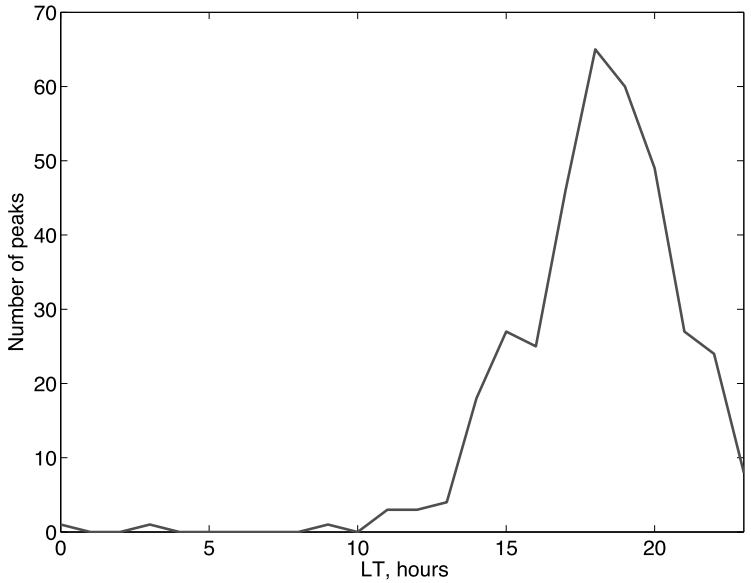

Figure 7. LT distribution of the deepest local Dxt minimum at any station at any time of storm for −100 nT storms in 1932–2009.

NOAA/POES satellites during a major storm [*Asikainen et al.*, 2005].

6. UT Distributions

[22] Figure 8 (top) depicts the UT distribution of storm-time local Dxt minima at each station for Dxt minimum less than −100 nT storms. Note that each station curve is the same as in Figure 5 but shifted in time corresponding to the station's longitude with respect to the Greenwich meridian (UT zero longitude). For example, HER UT distribution peaks at 18 UT since HER local time is one hour ahead of UT and the LT distribution at HER peaks at 19 LT (see Figure 5). The mean curve of the four UT distributions of Figure 8 (top) ("4-station mean") is depicted in Figure 8 (bottom) together with the UT distribution of global Dxt peaks ("Dxt peaks") and the hourly averages of the global Dxt index ("Dxt mean") during the same storms. All the three distributions in Figure 8 (bottom) depict a closely similar UT variation. As seen in Figure 8 (top), the two most closely located stations, HON and KAK, have their peak values at 05 UT and 09 UT, i.e., closer than any other pair of station maxima. On the other hand, the longest difference between the maxima of any two stations in Figure 8 (top) is between KAK and HER. The proximity of HON and KAK peaks leads to the morning maximum of the Dxt mean curve in Figure 8 (bottom), and the large separation between KAK and HER to the corresponding minimum around noon.

[23] As seen in Figure 8 (bottom) the UT distribution of hourly values of the global Dxt index ("Dxt mean") is clearly non-uniform. (A similar UT variation is found also for all Dxt values.) This variation has been suggested to be due to certain solar-terrestrial effects causing UT variability like the Russell-McPherron effect [*Russell and McPherron*, 1973]. However, the close similarity between the three curves in Figure 8 (bottom) demonstrates that the UT variation of the Dxt/Dst index is mainly due to the slightly inhomogeneous LT distribution of Dst stations, in agreement with earlier studies [*Takalo and Mursula*, 2001]. Accordingly, studies trying to find evidence on any external causes to such UT variation should take this deficiency into account.

[24] We have plotted in Figure 9 the distribution of UT time differences between the local Dxt minimum hour at the station that depicts the deepest (most disturbed) local storm-time Dxt index, and the global Dxt minimum hour. (In most cases, the station is close to 18 LT; see Figure 7.) Positive value of the time difference means that the station minimum is later than the global Dxt peak. The distribution is strongly peaked around zero, the difference being more than one hour only in about 26% of storms. This indicates that the timing of the global Dxt minimum, i.e., storm intensity, is mostly determined by the hour when one of the stations is at the site of maximum disturbance around 18 LT. This underlines the importance of this LT region because it strongly affects not only storm intensity but also the overall temporal evolution of storms, which is defined in terms of the global Dxt/Dst index. (Note also that the small asymmetry of the distribution in favor of local Dxt minimum at later UT hour indicates the spreading of the disturbed region.)

7. Local Time Asymmetries

[25] As is evident from the previous discussion (e.g., in Figures 5 and 7), the individual stations observe quite different disturbances depending mainly on their local time position. This leads to considerable storm-time local time asymmetry, whose amount varies, e.g., with storm phase and intensity. We have depicted in Figure 10 the distribution of the number of storms for different values of asymmetry, i.e., the difference between the weakest (highest Dxt) and deepest (lowest) local Dxt index at any of the four stations. (This definition gives a positive asymmetry.) All four intensity levels are treated separately in Figure 10. Figure 10a depicts the momentary asymmetries at the hour of the global Dxt minimum, while Figure 10b shows the asymmetry of local minima, i.e., the difference between the weakest and

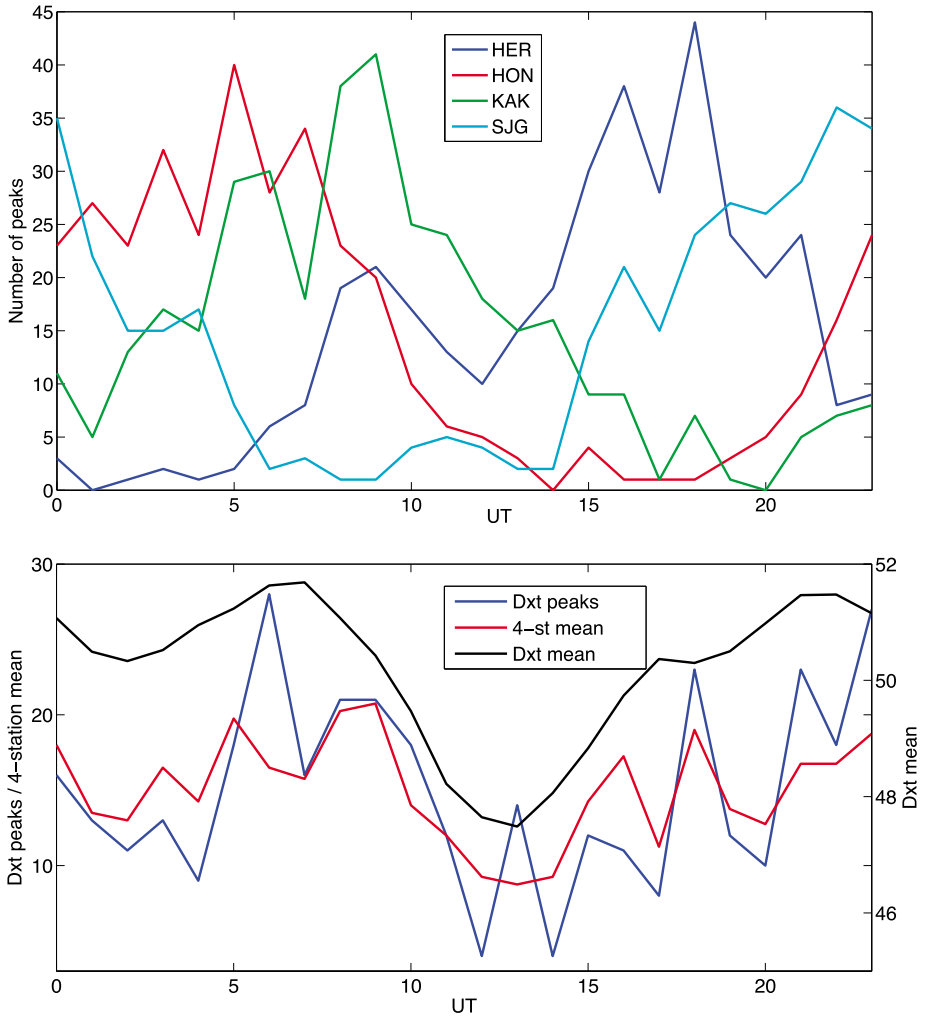

Figure 8. (top) UT distribution of storm-time local Dxt minima at each Dst station for Dxt minimum less than −100 nT storms. (bottom) Mean of the four local UT distributions ("4-station mean"; red line), UT distribution of global Dxt minima ("Dxt peaks"; blue line) and hourly averages of the global Dxt index ("Dxt mean"; black line) during the same storms.

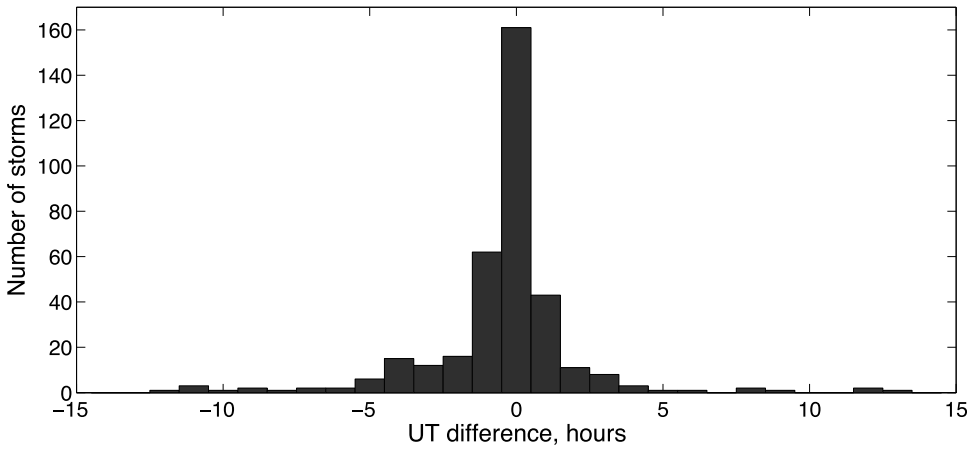

Figure 9. Histogram distribution of UT difference between the local Dxt minimum hour at the station that depicts the largest local Dxt index and the global Dxt minimum time during Dxt minimum less than −100 nT storms.

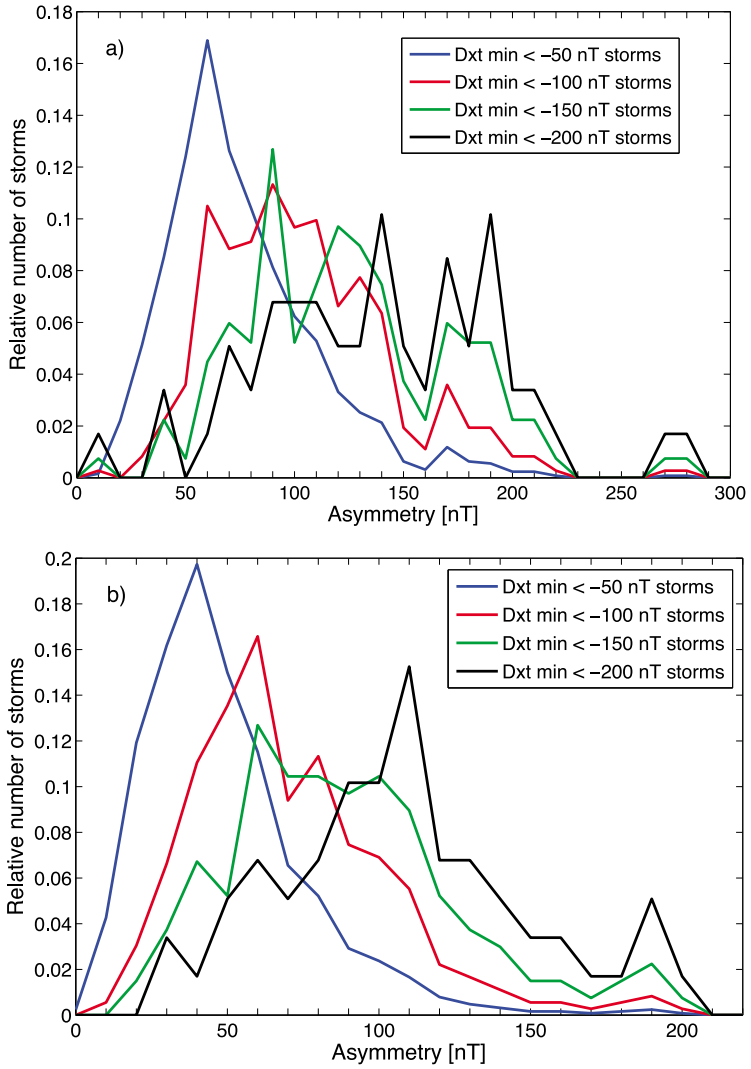

Figure 10. Distribution of relative number of storms as a function of local time asymmetry for the four intensity levels. (a) Momentary asymmetry at global Dxt minimum; (b) asymmetry of storm-time local Dxt minima. All distributions are normalized by the total number of storms of the respective intensity level.

deepest local storm-time minima. Note that all histograms have been normalized by the total number of storms of the respective intensity level in order to match the four distributions in one figure.

[26] Figures 10a and 10b show that the mode of the asymmetry distribution (i.e., the most common value of asymmetry) increased from about 70 nT or 50 nT, respectively, for Dxt < −50 nT storms to about 150 or 120 nT, respectively, for Dxt < −200 nT storms. However, the ratio between the typical asymmetry and the storm intensity level (the typical level of local disturbance) is larger for weaker than stronger storms, implying again that strong storms are relatively more symmetric than the weak storms. The weak storms include a large fraction of CIR driven storms whose typical intensity is only slightly below −50 nT [*Richardson et al.*, 2006]. On the other hand, most storms with Dxt minimum below −100 nT are CME driven storms. The momentary asymmetries are naturally somewhat larger than the asymmetries between local minima, since momentary Dxt indices also include rather weak values from the least disturbed stations, which increases the momentary asymmetry (see also Figures 4). However, the distributions extend in both cases until about 220 nT. (Very few storms have even larger momentary asymmetries up to almost 300 nT.) *Huttunen et al.* [2006] found asymmetries of about 72 nT and 112 nT for a sample of 14 magnetic cloud and 14 sheath driven CME storms of −100 nT intensity, respectively. Convincingly, the mode of the momentary asymmetry distribution for −100 nT storms, about 90 nT, is between the asymmetries for these two storm types. (Note also that the distributions in Figure 10a are fairly symmetric, in particularly for stronger storms, while the distributions in Figure 10b resemble more closely a lognormal distribution, probably because they are effectively constrained to be positive by definition.)

[27] Figure 11 shows the hourly SPE median curves, depicting the temporal development of the momentary asymmetry during storms of different intensity levels. SPE

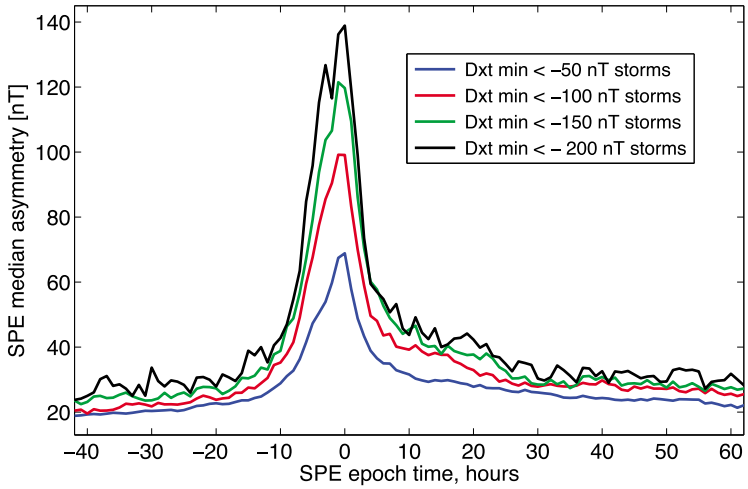

Figure 11. Superposed epoch median values of the hourly momentary asymmetry during storms of different intensity levels. SPE zero time is the global Dxt minimum time.

zero time is set to the time of global Dxt minimum. Figure 11 shows the increase of the median asymmetry at Dxt minimum with increasing storm intensity (see Figure 10a). At all storm levels, the asymmetry maximum is strongly peaked at zero epoch time (the end of the main phase defined by global Dxt minimum). The half-width of the asymmetry distribution remains roughly the same at all intensity levels, suggesting that the most disturbed ring current develops (increases and decays) roughly within the same time interval, irrespective of storm intensity. However, the rate of evolution (expressed in terms of nT/hour) is roughly twice faster for −200 nT storms. This difference is particularly clear during the early recovery phase of storm.

[28] Note also that the distribution in Figure 11 is asymmetric in two ways. First of all, slightly larger asymmetries are found during less than 9 hours before the SPE zero time than equally many hours thereafter. The early asymmetry of the distribution includes the effect of the pressure increases at the dayside before the storm onset and the development of the main disturbances at dusk sector during the storm main phase. (This asymmetry is relatively more pronounced in weak storms.) Secondly, about 10 hours away from the zero epoch time the asymmetry after zero time is at a higher level than before the zero time. This indicates that the asymmetry remains, on an average, at a notable level during the whole three-day interval included in this study.

[29] Finally, we have compared the hourly momentary asymmetry with the asymmetry parameter ASY-H developed at the Kyoto WDC [*Iyemori*, 1990]. This parameter is calculated from the H-component disturbance at six midlatitude stations (three in both hemispheres) at one-minute time resolution for 1981–2009. For comparison with our hourly estimate of asymmetry, we have constructed three different hourly ASY-H data sets taking the hourly maxima, minima and means of the 60 one-minute ASY-H values for each hour. Figure 12 depicts the scatterplot and best-fit correlation lines between the momentary asymmetry and the three simultaneous ASY-H series for Dxt minimum less than −100 nT storms over the same time interval 1981–2009. Despite large scatter, there is fair correlation between momentary asymmetry and the three ASY-H indices (correlation coefficients 0.63, 0.58 and 0.44 for ASY-H means, maxima and minima). However, there is a rather large intercept, and the correlation line slope for ASY-H mean is below one, about 0.68. These differences are probably due to the larger number of ASY-H stations, which allows to detect small local asymmetries better than with four stations. Therefore ASY-H mean is slightly larger than momentary asymmetry for storms with asymmetry of about −50 nT and smaller for storms with asymmetry −200 nT. The best agreement is for storms with asymmetry of about −100 nT. Finally, Figure 13 depicts the superposed epoch median values of the three hourly ASY-H indices and the momentary asymmetry for −100 nT storms in 1981–2009, using the global Dxt minimum time as the SPE zero time. The overall

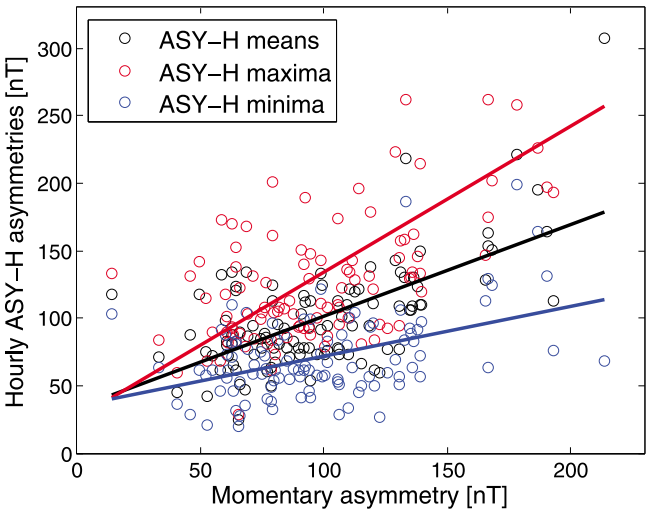

Figure 12. Scatterplot between the three hourly ASY-H indices and the momentary asymmetry during Dxt minimum less than −100 nT storms in 1981–2009. Best fit correlation lines are included.

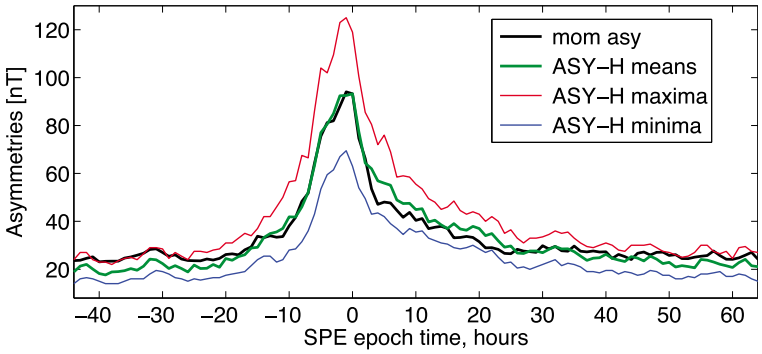

Figure 13. Superposed epoch median values of the three hourly ASY-H indices and the momentary asymmetry during Dxt minimum less than −100 nT storms in 1981–2009. SPE zero time is the global Dxt minimum time.

time evolution is very similar between the momentary asymmetry and the ASY-H mean.

8. Conclusions and Summary

[30] We have studied the properties of storms based on the unique database of global and local Dxt indices calculated for the four Dst stations in 1932–2009. We required that none of the four Dst stations should have any data gaps during five days around the Dxt minima of storms to be included in the study. This selection condition reduced the number of storms by 25% to 35% (increasing with storm intensity), but guaranteed a homogeneous set of indices during all storms. The database consists of 1268/362/134/59 storms in four intensity categories with global Dxt minimum less than −50/−100/−150/−200 nT.

[31] During these storms the global Dxt index minima were, on an average, −94/−156/−216/−275 nT, while the mean values of the deepest (most disturbed) local Dxt minima were −137/−214/−285/−350 nT. This implies that the deepest storm-time local Dxt indices are typically 31/27/24/21% below the global Dxt index minima. Maximum differences between the storm-time local Dxt minima can be much larger, up to about 200 nT. This emphasizes that the global Dxt/Dst index can seriously underestimate the severity of local disturbances. The difference between the global and local Dxt minima can also lead to erroneous conclusions about storm drivers or the simulation capabilities of storm models, if only trained based on global minima.

[32] The relative difference between global and local minima decreases with storm intensity, supporting the view that the stronger (mostly CME driven) storms are more symmetric than the weaker (mostly CIR related) storms. Asymmetries (and storm main phases) were found to develop (including increase and decay) roughly within the same time interval, irrespective of storm intensity. However, the rate of evolution, especially the decay, is roughly twice faster for large storms. Large storms are marked by the fact that all local time sectors become very disturbed by the end of the storm main phase, leading to relatively more symmetric spatial distribution.

[33] We discussed two sample storms, which depicted the spatial distribution and temporal evolution of local disturbances at the four Dst stations. Notable differences were seen between the two storms of different origin and intensity level, with the larger CME driven storm evolving faster and relatively more symmetrically than the CIR driven storm. The location of the largest disturbance for each storm (and even each injection) is found in the late afternoon sector at about 18 LT. The statistical LT distribution was shown to be very steep both toward the dayside and the night side, with the ratio of Dxt minima at 18LT and at 00LT being more than 6, challenging the idea of ions originating mainly in the midnight sector.

[34] We showed that the time of the global Dxt minimum is mostly determined by the hour when one of the stations is at the site of maximum disturbance around 18 LT. This further emphasizes the importance of this LT region because it determines the storm intensity level and also strongly affects the overall temporal evolution of storms. We studied the relative timing of local minima statistically and found that the earlier LT hour stations observed their minimum a couple of hours after the deepest minimum, in agreement with westward drift of ions. Typically, ions drift about 5 LT hours in about 2 hours in the afternoon LT sector. Although the statistical distributions of time differences agree with westward drift of ions, the intensities are larger in the afternoon LT sector.

[35] Concluding, the local Dxt indices have proven to be useful in studying the average properties of storms, in particular in describing the spatial distribution and temporal evolution of storms.

[36] **Acknowledgments.** We acknowledge the financial support by the Academy of Finland to projects 131350, 128189 and 137054, the Center for International Mobility (grant TM-09-6353), and the Thule Institute of the University of Oulu. The research leading to these results has received funding from the European Commission's Seventh Framework Programme (FP7/2007-2013) under the grant agreement 218816 (SOTERIA project, www.soteria-space.eu). The work at SINP MSU was partly supported by RF State Project (N 07.514.11.4020).

[37] Masaki Fujimoto thanks the reviewers for their assistance in evaluating this paper.

References

Asikainen, T., R. Kerttula, K. Mursula, R. Friedel, D. Baker, F. Soeraas, J. Fennell, and J. Blake (2005), Global view of energetic particles during a major magnetic storm, in *The Inner Magnetosphere: Physics and Modeling*, *Geophys. Monogr. Ser.*, vol. 155, edited by T. Pulkkinen, N. Tsyganenko, and R. Friedel, pp. 97–104, AGU, Washington, D. C.

Burton, R. K., R. L. McPherron, and C. T. Russell (1975), An empirical relationship between interplanetary conditions and Dst, *J. Geophys. Res.*, *80*, 4204–4214.

Buzulukova, N., M.-C. Fok, A. Pulkkinen, M. Kuznetsova, T. E. Moore, A. Glocer, P. C. Brandt, G. Tóth, and L. Rastätter (2010), Dynamics of ring current and electric fields in the inner magnetosphere during disturbed periods: CRCM-BATS-R-US coupled model, *J. Geophys. Res.*, *115*, A05210, doi:10.1029/2009JA014621.

Campbell, W. H. (1996), Dst is not a pure ring current index, *Eos Trans. AGU*, *77*(30), 283–285.

Campbell, W. H. (2004), Failure of Dst index fields to represent a ring current, *Space Weather*, *2*, S08002, doi:10.1029/2003SW000041.

Cash, M. D., R. M. Winglee, and E. M. Harnett (2010), Storm time production of ring current ions: Variations in particle energization and injection with ionospheric source region, *J. Geophys. Res.*, *115*, A00J12, doi:10.1029/2010JA015759.

Echer, E., W. D. Gonzalez, B. T. Tsurutani, and A. L. C. Gonzalez (2008), Interplanetary conditions causing intense geomagnetic storms (Dst ≤ -100 nT) during solar cycle 23 (1996–2006), *J. Geophys. Res.*, *113*, A05221, doi:10.1029/2007JA012744.

Gonzalez, W. D., B. T. Tsurutani, and A. L. Clúa de Gonzalez (1999), Interplanetary origin of geomagnetic storms, *Space Sci. Rev.*, *88*, 529–562.

Gopalswamy, N. (2010), The CME link to geomagnetic storms, in *Proceedings of IAU Symposium*, vol. 264, edited by A. G. Kosovichev, A. H. Andrei, and J.-P. Rozelot, pp. 326–335, Int. Astron. Union, Paris, doi:10.1017/S1743921309992870.

Huttunen, K. E. J., H. E. J. Koskinen, A. Karinen, and K. Mursula (2006), Asymmetric development of magnetospheric storms during magnetic clouds and sheath regions, *Geophys. Res. Lett.*, *33*, L06107, doi:10.1029/2005GL024894.

Iyemori, T. (1990), Storm-time magnetospheric currents inferred from mid-latitude geomagnetic field variations, *J. Geomagn. Geoelectr.*, *42*, 1249–1265.

Jordanova, V., H. Matsui, P. Puhl-Quinn, M. Thomsen, K. Mursula, and L. Holappa (2009), Ring current development during high speed streams, *J. Atmos. Sol. Terr. Phys.*, *71*, 1093–1102, doi:10.1016/j.jastp.2008.09.043.

Kalegaev, V. V., K. Y. Bakhmina, I. I. Alexeev, E. S. Belenkaya, Y. I. Feldstein, and N. V. Ganushkina (2008), Ring current asymmetry during a magnetic storm, *Geomagn. Aeron.*, *48*, 747–758, doi:10.1134/S0016793208060078.

Kamide, Y., and Y. P. Maltsev (2007), Geomagnetic storms, in *Handbook of the Solar-Terrestrial Environment*, edited by Y. Kamide and A. C.-L. Chian, pp. 356–373, Springer, New York.

Karinen, A., and K. Mursula (2005), A new reconstruction of the Dst index for 1932–2002, *Ann. Geophys.*, *23*, 475–485.

Karinen, A., and K. Mursula (2006), Correcting the Dst index: Consequences for absolute level and correlations, *J. Geophys. Res.*, *111*, A08207, doi:10.1029/2005JA011299.

Karinen, A., K. Mursula, J. Takalo, and T. Ulich (2002),An erroneous Dst index in 1971, in *Solspa 2001, Proceedings of the Second Solar Cycle and Space Weather Euroconference*, edited by H. Sawaya-Lacoste, *ESA Spec. Publ.*, *477*, 443–446.

Le, G., C. Russell, and K. Takahashi (2004), Morphology of the ring current derived from magnetic field observations, *Ann. Geophys.*, *22*, 1267–1295, doi:10.5194/angeo-22-1267-2004.

Lepping, R. P., et al. (2001), The Bastille day magnetic clouds and upstream shocks: Near-Earth interplanetary observations, *Sol. Phys.*, *204*, 285–303, doi:10.1023/A:1014264327855.

Liemohn, M. W., J. U. Kozyra, M. F. Thomsen, J. L. Roeder, G. Lu, J. E. Borovsky, and T. E. Cayton (2001), Dominant role of the asymmetric ring current in producing the stormtime Dst*, *J. Geophys. Res.*, *106*, 10,883–10,904.

Love, J. J., and J. L. Gannon (2009), Revised Dst and the epicycles of magnetic disturbance: 1958–2007, *Ann. Geophys.*, *27*, 3101–3131.

Lui, A. T. Y., R. W. McEntire, and S. M. Krimigis (1987), Evolution of the ring current during two geomagnetic storms, *J. Geophys. Res.*, *92*, 7459–7470.

Lyons, L. R., and D. J. Williams (1984), *Quantitative Aspects of Magnetospheric Physics*, D. Reidel, Dordrecht, Netherlands.

Mursula, K., L. Holappa, and A. Karinen (2008), Correct normalization of the Dst index, *Astrophys. Space Sci. Trans.*, *4*, 41–45.

Mursula, K., L. Holappa, and A. Karinen (2011), Uneven weighting of stations in the Dst index, *J. Atmos. Sol. Terr. Phys.*, *73*, 316–322.

Richardson, I. G., et al. (2006), Major geomagnetic storms (Dst ≤ -100 nT) generated by corotating interaction regions, *J. Geophys. Res.*, *111*, A07S09, doi:10.1029/2005JA011476.

Russell, C. T., and R. L. McPherron (1973), Semiannual variation of geomagnetic activity, *J. Geophys. Res.*, *78*, 92–108.

Sugiura, M. (1964), Hourly values of equatorial Dst for the IGY, *Ann. Int. Geophys. Year*, *35*, 9.

Sugiura, M., and T. Kamei (1991), Equatorial *Dst* index 1957–1986, in *IAGA Bulletin*, vol. 40, edited by A. Berthelier and M. Menvielle, ISGI Publ. Off., Saint-Maur-des-Fossés, France.

Takalo, J., and K. Mursula (2001), A model for the diurnal UT variation of the Dst index, *J. Geophys. Res.*, *106*, 10905–10914.

Tsurutani, B. T., and W. D. Gonzalez (1997), *The Interplanetary Causes of Magnetic Storms: A Review*, pp. 77–90, AGU, Washington, D. C.

Tsurutani, B. T., et al. (2006), Corotating solar wind streams and recurrent geomagnetic activity: A review, *J. Geophys. Res.*, *111*, A07S01, doi:10.1029/2005JA011273.

Weygand, J. M., and R. L. McPherron (2006), Dependence of ring current asymmetry on storm phase, *J. Geophys. Res.*, *111*, A11221, doi:10.1029/2006JA011808.

Williams, D. J. (1987), Ring current and radiation belts, *Rev. Geophys.*, *25*, 570–578.

Xu, Z., L. Zhu, J. Sojka, P. Kokoszka, and A. Jach (2008), An assessment study of the wavelet-based index of magnetic storm activity (wisa) and its comparison to the Dst index, *J. Atmos. Sol. Terr. Phys.*, *70*, 1579–1588, doi:10.1016/j.jastp.2008.05.007.

Zhang, J., et al. (2007), Solar and interplanetary sources of major geomagnetic storms (Dst ≤ -100 nT) during 1996–2005, *J. Geophys. Res.*, *112*, A10102, doi:10.1029/2007JA012321.

L. Holappa, A. Karinen, and K. Mursula, Department of Physics, University of Oulu, FI-90014 Oulu, Finland. (kalevi.mursula@oulu.fi)

I. S. Veselovsky and O. S. Yakovchouk, Institute of Nuclear Physics, Moscow State University, 119991 Moscow, Russia.